Emission of titanium dioxide nanoparticles from building materials to the environment by wear and weather

Neeraj Shandilya, Olivier Le Bihan, Christophe Bressot, Martin Morgeneyer

Emission of Titanium Dioxide Nanoparticles from Building Materials to the Environment by Wear and Weather

*Neeraj Shandilya, Olivier Le Bihan, Christophe Bressot, Martin Morgeneyer**

Neeraj Shandilya, Dr. Olivier Le Bihan, Dr. Christophe Bressot
Institut National de l'Environnement Industriel et des Risques (INERIS), Parc Technologique Alata BP 2, 60550 Verneuil-en-Halatte, France

E-mail: martin.morgeneyer@utc.fr

Neeraj Shandilya, Dr.-Ing. Martin Morgeneyer
Université de Technologie de Compiègne (UTC), rue Roger Coutollenc, 60200 Compiègne, France

Abstract

In the present work, we investigate the effect of the weathering duration on a commercial photocatalytic nanocoating on the basis of its nanoparticles emission tendency into the two media - air and water. It is found that the increase in the weathering duration results into the stepwise structural deterioration of the nanocoating which, in turn, decreases the nanocoating life, changes the nanocoating removal mechanism and increases the particle emission concentration. The emission of the free TiO_2 nanoparticles is found to be weathering duration dependent. Three quantities- Emission Transition Pace (ETP), Stable Emission Level (SEL) and Stable Emission Duration (SED) are introduced. By linearly extrapolating these quantities from short weathering durations, the complete failure of the nanocoatings can be predicted and moreover the potential increase of nanoparticles release into the air.

Keywords: Weathering, Emission, Nanocoating

Abstract Art

1. Introduction

Photocatalytic nanocoatings are readily being applied on the external walls of buildings for their anti bacterial and self cleaning properties.[1, 2] These properties are ensured by the presence of embedded manufactured photocatalytic titanium dioxide (TiO_2) nanoparticles in the coating matrix. Resting on the external surfaces, these nanocoatings are frequently subjected to various mechanical solicitations and environmental weathering in real life conditions. [3, 4, 5] As a result, the consequent loss in their structural integrity leads to their disintegration which, in turn, may lead to the exposure of embedded nanoparticles [6] and thus their possible release too. Depending upon the type of medium in contact, this release can be into air as well as into ground waters. For a durable development, understanding their ecological and human health effects is important. In the last decade, slowly though, this concern has started gaining attention.[6-19] In this context, various toxicological and ecotoxicological studies have also demonstrated toxic effects of some types of TiO_2 nanoparticles.[20-25]

Here, the nanoparticles release from a commercial photocatalytic nanocoating is evaluated as a function of the duration of its weathering. Whilst the nanoparticles emission into air is studied via abrasion tests, their emission into water is studied via the microscopy and leaching tests of runoff samples. Through microscopic studies of the intermediate degraded states of the coated surfaces, the particles emission is shown to be weathering duration dependent.

2. Materials and Methods

2.1. Samples

For the study, a commercially available photocatalytic nanocoating, PHOTOCAL MASONRY, was chosen. It is manufactured by NANOFRANCE Technologies, France. It consists of anatase titanium dioxide nanoparticles having a primary size of <8 nm and a

volume percentage of 1.1%. Other material properties are as follows- Coagulation Index: ~2; Appearance: white; Dispersant: Polymethylmethacrylate (PMMA). This type of nanocoating is fabricated specifically for the applications on porous surfaces like brick, concrete etc. The substrate chosen for the nanocoating application was a masonry brick (11 cm x 5 cm x 5 cm; Leopard brick, Ref: 901796, Castorama, France). It is basically an alumino-silicate brick which is frequently used in constructing façades, house walls, stairs etc. The microscopic analysis of the nanocoating and the substrate were carried out using Optical Microscope (Model Imager.M1m; Carl Zeiss MicroImaging GmbH; Germany), Energy Dispersion Spectroscopy (EDS; Model X-max; Oxford Instruments UK) and Transmission Electron Microscope (TEM; Model CM12; Philips, The Netherlands). Information on the microscopic analysis results are provided in the separately available *supplementary part* of this paper. Four coating layers with a total thickness of 80 µm approx. were applied on the brick substrates. The substrate surfaces were prepared and the nanocoating was applied following the guidelines in the technical data sheet recommended by the nanocoating manufacturer (i.e. degreased using brush and ethanol soaked paper, dry and dust free surfaces; use of a High Volume Low Pressure spray during coating; 25°C of ambient temperature).

2.2. Artificial weathering

The artificial weathering tests were performed with the nanocoated and the uncoated reference brick samples in a weathering chamber (Model Suntest XLS+; Atlas; Germany). The artificial weathering consisted of maximum 2658 cycles (which corresponds to 7 months) of 2 hours each (120 min of UV light, 102 min dry, 18 min water spray). A xenon arc lamp (300–400 nm; 60 W/m^2; Model NXE 1700; Ametek SAS; France) with an optical radiation filter was used as the UV source. Such a system is a representative of natural sunlight.[20] The temperature during UV exposure was monitored and averaged at 38 °C. The conditions were

chosen on the basis of an international standard.[26] De-ionized and purified water (conductivity < 1 µS/cm) was used for the water spray onto the nanocoated samples. The runoff water was collected in a reservoir, mounted at the bottom of the climate chamber. The whole weathering process was intervened at selected times (2, 4, 6 and 7 months) for analyzing the in-process condition of the test samples and sampling the collected runoff water for its leaching analysis.

2.3. Leaching

To quantify the TiO_2 content in the leachate water, fixed amounts of samples (100 ml) were collected at selected times (as indicated earlier) and analyzed by using Inductively Coupled Plasma Mass Spectrometry (ICP-MS; Model 7500cx; Agilent Technologies; USA). The operating conditions of the ICP-MS were as follows- Sample volume: 2 ml; RF Power: 1550 W; RF Matching: 1.78 V; Carrier Gas: 0.85 l/min; Makeup gas: 0.2 l/min; Nebulizer: Micromist; Nebulizer pump: 0.1 r/s; S/C temperature: 15 °C; He flow rate: 5 ml/min; H_2 flow rate: 2 ml/min; Integration time: 0.1 s; Chamber & Torch: Quartz; Cone: Ni; Element detection threshold limit: 0.5 µg/l.

2.4. Abrasion

A modified Taber™ linear abrasion apparatus (Model 5750; Taber Inc. USA) [27] was used for the abrasion of the nanocoated samples. The standard form of this apparatus is referenced in numerous internationally recognized test standards.[28-30] This apparatus is already being used in industries for analyzing the performance of products like paint, coating, metal, paper, textile etc., during the application of a mechanical stress.[31] The normal stress of the abradant of about 15 – 500 kPa, being applied through Taber, also corresponds to the typical normal- and thus tangential- stress levels applied to surface coatings in a domestic setting, e.g. walking

with shoes, displacement of different furnishings etc.[3, 32] It incorporates a motor driven horizontal arm (bar) that displaces an abradant in a back and forth linear motion over the test sample. The abrasion is caused by the friction at the contact surface between the surfaces of the abradant and the sample. Via a vertical shaft, a known weight is mounted on the top of the abradant which shall be referred to as the *Normal Load* in the following text. The Taber™ H38 non-resilient vitrified clay-carborundum abradant was used during the abrasion of the nanocoated samples. This abradant comes in a cylindrical shape (6 mm diameter, 2 cm length) and comprises of very fine abrasive particles (~4 µm) of carborundum that provide mild abrasion. For reproducing the domestic stress conditions, a normal load of 6 N was chosen. An abrasion stroke length of 76 mm, abrasion speed of 60 cycles/min and abrasion duration of 10 min were other selected parameters.

2.5. Experimental set-up

Figure 1 shows the scheme of the complete experimental set-up. Particle free air is passed through a nanosecured work post (HPPE 10, Erma Flux S.A., France) containing the Taber abrasion apparatus. Already been successfully employed in various nanoparticles' dustiness tests,[33] this work post has a particle filter efficiency of 99.99%. The air flow rate inside this work post is equal to 31000 l/min. The test sample is placed inside a self designed *Emission Test Chamber* (0.5 m x 0.3 m x 0.6 m).[34] A small fraction of the air circulating inside the nanosecured work post passes through the emission test chamber before starting the abrasion tests in order to make it free from background particles. As soon as the chamber becomes particle free, it is sealed completely. A slot is also provided on one of the walls of this chamber allowing the horizontal arm of the abrasion apparatus passing through and operating the motor unit placed externally. A radial symmetric sampling hood with a volume of 713 cm^3 provides an encapsulation of the sampling suction zone around the abradant. Such sampling

hood has also been employed in other studies with varying volumes, such as 1500 cm^3 by Vorbau et al.[3] and 60 cm^3 by Gohler et al.[35]. Its use minimizes particle loss to the emission test chamber's walls or other surfaces. Furthermore, the aerosol concentration remains relatively high due to the low volume of the sampling hood and the fixed total sample flow that amounts to 6.8 l/min. The Taber apparatus along with the emission test chamber constitute the Aerosol Generation Section (*AGS*). The *AGS* is connected to an Aerosol Measurement Section (*AMS*) using anti-static electrically conductive tubes (6 mm diameter) where the generated aerosol particles are characterized in terms of their number concentration and size distribution. The particle number concentration (*PNC*) can be defined as the number of particles present in a unit centimeter cube of air at a given instant of time. The particle size distribution (*PSD*) is the classification of the PNC according to their size. The instruments used to measure these two quantities were: Condensation Particle Counter (CPC), Scanning Mobility Particle Sizer (SMPS), Aerodynamic Particle Sizer (APS) and a Mini Particle Sampler (MPS®; Ecomesure Inc. France).[36] The details on these instruments and their operation conditions are shown in figure 1. Whilst the CPC measures the emitted aerosol particles number concentration (EAPNC), the PSD is measured using SMPS and APS. A MPS is used for the particle collection through filtration technique on copper mesh grids which can be used later in TEM for various qualitative analyses of the emitted aerosol particles without any limitation on the aerosol size. Therefore, the whole aerosol measurement section, quantifying the particle emission, can measure aerosol particles having sizes ranging from 4 nm to 20 µm.

2.6. Background and particle loss

Three empty test runs were done before the main abrasion experiment to measure the concentration of the background particles and those generated by the motor in abrasion

apparatus. Without the test sample present in the chamber, the average concentration, detected by CPC within the sampling hood, was ~ 0.7 cm^{-3} with a standard deviation of 0.2 cm^{-3}. Therefore, the concentrations of all the background particles and those generated by the abrasion apparatus were insignificant. The calculations on the loss of particle concentration, due to their deposition on the walls of the chamber, have shown a loss of 4% in number during 10 min (i.e. the duration of the abrasion process).

For the present experimental set-up, the particle loss in the connecting tubes (i.e. losses due to their gravitational settling, inertial deposition etc.) has been calculated by Shandilya et al. [37] on the basis of system of equations enlisted by Brockmann et al. [38] Shandilya et al.[37] found it to be 17% for particles having size less than or equal to 10 nm. For the 100 nm sized particles or bigger, the loss reduces to mere 1%.

3. Results and Discussion

3.1. Structural deterioration of nanocoated sample surfaces

In figure 2 (a) to (e), the evolution in the surface deterioration of the nanocoated sample can be observed with the increase in weathering duration. The optical microscopic image of a non-weathered sample (figure 2 (a)) shows a continuous and intact form. With 2 months of weathering (figure 2 (b)), *ridges* and *valleys* start to appear on the surface. If the weathering continues, they develop into the cracks by 4 months of weathering (figure 2 (c)). After 6 months, these cracks start to broaden up with branching at different parts (figure 2 (d)). By 7 months, the nanocoating is no longer continuous but reduced in the form of *lumps* (figure 2 (e)). On the contrary, for an uncoated reference sample, no such effect of weathering was observed throughout the whole process. In the literature, the cracking of water based nanocoatings (as in present case) has been attributed mainly to two factors: drying stress due to water content evaporation [39-42] and gradual embrittlement of the polymeric binder present

in the nanocoating during its interaction with UV rays.[43] Moreover, the cracking is often accompanied by the shrinking or compaction of the nanocoating on the surface due to the evaporation of the water content, as observed by Murray [40] and Dufresne et al. [41]

The nanocoating's shrinking and cracking may result in the exposure of the brick surface, lying underneath. In order to confirm this hypothesis, EDS analysis of the weathered nanocoated sample surfaces was done to create an elemental map between Ti (contributed by the nancoating) and Ca (contributed by the brick). This would show the change in completely exposed surfaces of the brick substrate. The results are shown in figure 2 (f) to (j). One may see that while the Ti content on the surface remains approximately the same throughout the weathering (average value ~16.1%), the Ca content and the exposed surface increase proportionately. It directly implies the shrinkage of the nanocoating with weathering. If continued further, the increased shrinking may even lead to the increase in Ti % density in the nanocoating lumps.

3.2. Particles emission into water by leaching

For measuring the emission of TiO_2 nanoparticles in the water, 100 ml of leachate samples were taken from the collected runoff water at selected times from a reservoir which was kept beneath the nanocoated samples. For a detection threshold of 0.5 µg/l of an element, Ti was found to be always below this threshold in the sample volume whereas the leached amount of Ca (contributed by the brick) was found to be proportionally increasing with the weathering duration. The TEM and EDS analysis of various droplets from the leachate samples (test methodology and results described in supplementary information) showed irregularly shaped *microsized* particle agglomerates.

In coherence with the ICP-MS measurements, the EDS analysis of these particle agglomerates also showed an overall increasing Ca content, from 3 to 17% (by mass), with weathering. A

meager Ti content (0.2-1%, by mass) was observed in all particle agglomerates. The C content (from nanocoating copolymer) was found to be varying from 3 to 10 % by mass. The other dominating elements were Si (~32%, by mass) and Al (~20%, by mass). An increased water conductivity (from <1 to 13 µS/cm) was also observed in the leachate samples which is supposed to be a consequence of the increased presence of Si, Al and Ca.

This concludes that despite the deterioration by weathering, the nanocoated sample surfaces are still strong enough to resist the leaching of the constituent nanoparticles in the runoff water. Infact, it is the brick that obviously leaches its constituents in the runoff water. These results seem to be consistent with Al-Kattan et al. [10] which studied the release of Ti, from paints containing TiO_2 nanoparticles, into runoff water under the effect of artificial weathering. They showed a close to background release of Ti, indicating that TiO_2 nanoparticles are strongly bound in the paint.

3.3. Particles emission into air by abrasion

Both uncoated reference and nanocoated samples were abraded after they were exposed to weathering with varying durations. In figure 3 (a) and (b), TEM images of the emitted aerosol particles are shown which were sampled and collected on mesh grids during the first 2 minutes of abrasion of the 4 and 7 months weathered nanocoated samples, respectively, under the same sampling conditions. More aerosol particles get deposited on the mesh grids when the weathering duration is increased from 4 to 7 months. When zoomed, irregularly shaped polydispersed aerosol particles with no specific evolution in the shape, over the variation of the weathering duration, were observed. Most importantly, for 7 months weathered nanocoated samples, the presence of a considerable amount of free nanoparticles of TiO_2 (Ti mass > 90%) was observed (figure 3 (c) & (d)). Since this result is in contrary to the findings of numerous studies [4, 31, 35, 44], it is of more particular interest as these studies show that a large

fraction of the emitted nanomaterial is present in the matrix-bound form and not in the free state. The increase in the relative % density of Ti, during the shrinking of the nanocoating with the weathering, (as hypothesized earlier) may lead to the generation of these free TiO_2 nanoparticles.

The results on the chemical composition of the aerosol particles, generated from the abrasion of 4 and 7 months weathered nanocoated samples, are shown in figure 3 (e). In this figure, the average mass percentages of 3 elements- C (essentially coming from the nanocoating's copolymer), Ti (essentially coming from the nanocoating) and Ca (essentially coming from the brick)- are shown. One can observe a sharp drop in the relative C content (from 56% to 12%) while a sharp rise in the relative Ti content (from 7% to 55%) when the weathering duration increases from 4 months to 7 months. Also, the relative Ca content, which is absent in the case of 4 months weathered nanocoated samples, starts appearing and attains a value of 6% with 7 months of weathering. Hence, a direct impact of the weathering duration on the size and chemical composition of the aerosol particles can be observed from these results. Moreover, the chances of the exposure of free TiO_2 nanoparticles are much higher in the case of 7 months weathered nanocoated samples.

The results on the EAPNC and PSD, measured within the volume of the sampling hood, are shown in figure 4. In figure 4 (a) and (b), the abrasion test starts at t=120 s and ends at t= 720 s. Before and after this time interval (i.e. t=0 to 120 s and t=720 to 840 s), the abrasion apparatus is at rest. For the uncoated reference samples, a constant EAPNC (~500 cm^{-3}; std. deviation: 5 to 16 cm^{-3}; repeated thrice) is observed, regardless the weathering durations. Hence, the artificial weathering has no apparent effect on the emitted aerosol particles from the uncoated reference sample. However, for the nanocoated samples, the EAPNC increases with the weathering duration. Except for 6 and 7 months, the nature of its variation with time

is also strikingly similar i.e. ascends initially, becomes constant, ascends again and becomes constant at last (the PSD, during the first constant phase, is shown in figure 4(d)).

For 6 and 7 months weathered nanocoated samples, we observe a rise in the EAPNC curves during their initial phases (t= 120 s to t= 360 s) beyond the maximum level observed for the shorter weathering durations. After t= 360 s, these curves tend back to the same level as that of the uncoated reference and their counterparts. Such a behavior can be explained on the basis of the nanocoating removal mechanism during the abrasion of the weathered nanocoated samples. In case of non-weathered, 2 and 4 months weathered nanocoated samples, the dominant material removal mechanism is assumed to be *abrasion wear* of the nanocoating due to its continuous and stable form. But for 6 and 7 months weathered nanocoated samples, it is hypothesized that the dominant material removal is rather *uprooting* of the nanocoating lumps (or soon to be lumps) by the abradant. Since these lumps are loosely attached to the surface, their uprooting is faster and easier. As a result, the EAPNC reaches its highest level as soon as the abrasion starts and comes back to the same level, later, as that of the uncoated reference, when all the nanocoating lumps have been uprooted and the brick surface is completely exposed. The PSD, shown in figure 4 (c) and (d) for uncoated reference and nanocoated samples respectively, vary in a different manner with respect to each other. Whilst for the uncoated reference samples, there is no significant change in the size mode (alternating between 250 nm to 350 nm) and maximum PNC (lying around 375 cm^{-3}, std. dev.: 0.2 to 8 cm^{-3}), a continuous evolution can be observed in these two parameters in case of the nanocoated samples.

Coming back to the nature of the EAPNC variation with time, as observed in figure 4 (b), an analytic model had been presented by Shandilya et al. [46] which approximates such a variation in terms of 4 phases for the present nanocoating and one other commercial one: Tipe® E502, TitanPE Technologies, Inc. (see figure 5). When an uncoated reference sample is abraded

(figure 4 (a)), the EAPNC reaches a maximum limit swiftly (represented by segment **EF** in figure 5(a); named as *phase I*) and then remains constant until the end of the abrasion (represented by segment **FI** in figure 5(a); named as *phase IV*). However, the EAPNC, in case of a nanocoated sample (figure 4 (b)), passes through two intermediate phases (represented by segments **FG** & **GH** in figure 5(b); named as *phases II* and *III* resp.) before becoming constant at the end i.e. *phase IV*. Obviously, for an uncoated surface, the phases II and III are absent in the evolution of the EAPNC.

If physically interpreted, the *phase I* is contributed by the evolution of the contact surface conditions between the abradant and the nanocoated sample surface when the abrasion starts. During this phase, an ascending EAPNC is observed. In *phase II*, the EAPNC is constant and the abrasion of the nanocoated sample surface takes place under a stable state. The nanocoating is getting removed gradually or slowly through its abrasion wear. The duration of this phase also signifies the apparent nanocoating life. By the end of *phase II*, the surface nanocoating layer is no more stable and just the nanocoating-brick interface is left. With the advent of *phase III*, the brick surface starts to get exposed gradually and by the end of this phase, it is completely exposed. Therefore, the EAPNC, during *phase IV*, arrives at the same level as that of an uncoated reference sample and remains constant afterwards.

Three quantities:

(i) **Emission Transition Pace (*ETP*)** i.e. $(\Delta C/\Delta t)_I$;

(ii) **Stable Emission Level (*SEL*)** i.e. $(\#C)_{II}$*;*

(iii) **Stable Emission Duration (*SED*)** i.e. T_{II}

can also be identified from figure 5 (a) and (b) and are discussed in the following. These are the important indicators for assessing the nanocoating useful life and EAPNC. In figure 6 (a) and (b), they are plotted as a function of the weathering duration. In figure 6 (a), we see that the ***ETP*** (defined as the rate of change of the EAPNC) increases with weathering duration for

weathered nanocoated samples whereas for the uncoated reference, it remains constant. Moreover, *ETP* values for non-weathered, 2 and 4 months weathered nanocoated samples lie beneath the uncoated reference sample. But for 6 and 7 months weathered nanocoated samples, they lie above. On the basis of figure 2 and 4, we have already hypothesized a change in the nanocoating removal mechanism during the transition of the weathering duration from 4 to 6 months. Therefore, one may conclude that if the *ETP* value of the EAPNC, from a nanocoated sample, lies beneath the one corresponding to its uncoated reference substrate, the nanocoating removal mechanism is dominated by the abrasion wear. If opposite, the uprooting of the nanocoating is more dominant. Under given abrasion conditions, if *ETP* does not increase with the weathering duration (as observed in case of the uncoated reference), it implies no change in the abrasion conditions, regardless of the weathering duration. But if it increases (as observed in case of the weathered nanocoated samples), it implies the change in the abrasion conditions. In the present case, such a change is imparted by the deterioration of the nanocoating, as shown, qualitatively, in figure 2. The second quantity, ***SED***, is a direct indicator of the nanocoating life - higher the *SED*, higher is the nanocoating life time. It appears to decrease with the weathering duration (figure 6 (b)). When SED= 0, it means that the nanocoating disappears as soon as its abrasion starts. Quantitatively, it allows extrapolating the effect of the shorter weathering durations to that of the longer ones without prolonging the weathering test in reality. In figure 6 (b), if the SED average values, from first 2 months of weathering, are extrapolated, we observe that SED reduces to 0 in 11 months. The extrapolation of the extreme limits (i.e. through maximum value of SED for 0 months and minimum value of SED for 2 months) can be used to calculate the minimum useful life of the nanocoating under present weathering conditions. If it is done in the present case, we observe that SED reduces to 0 in 6 months- this is exactly what we observe in the figure 6 (b). Moreover, the average value of *SED* is decreasing from 320 s to

110 s (i.e. a reduction factor of ~3) in mere first 4 months of weathering. The EAPNC during SED is equal to ***SEL***. In figure 6 (b), it appears to increase with the weathering duration. Since SED= 0 for 6 and 7 months of weathering, therefore, SEL value for these durations cannot be calculated.

If summarized, we can say that under the present experimental conditions, a step-wise and complete surface deterioration of the nanocoated samples was observed as a function of the duration of a weathering by UV, temperature and water. This surface deterioration led directly to an increase of the emitted aerosol particles number concentration (measured within the volume of the sampling hood) and the TiO_2 content of the aerosolized wear particles. A considerable presence of free TiO_2 nanoparticles was observed in the case of the 7 months weathered nanocoated samples. This was a fundamental change observed in the chemical composition of the aerosol particles, as for short weathering durations, TiO_2 nanoparticles were always found to be embedded inside the released coarse wear particles with a polymeric matrix. This increase might still continue for longer weathering durations. With a high specific surface area, these free nanoparticles aerosols now accentuate a potential risk in terms of nano- toxicity. In case of leaching, no such effects were observed during 7 months of weathering. However, fears still remain on how and in what concentrations the leaching of TiO_2 might occur during prolonged weathering durations. This study also proposed an outline to understand the phenomenon of aerosolization and the indicators, like *Emission Transition Pace*, *Stable Emission Level* and *Stable Emission Duration*, for its monitoring. They were found to be significant to quantitatively predict the emitted aerosol particles number concentration and nanocoating useful life by the means of linear extrapolation from shorter weathering durations. It is possible to extend this study to a broad spectrum of nanocoatings, with the prospect of seeking their optimal formulations on the basis of nano risk i.e. emissions control.

Acknowledgements

This work has been carried out in the framework of the Labex SERENADE (ANR-11-LABX-0064) and the A*MIDEX project (ANR-11-IDEX-0001-02), funded by the French Government program, Investissements d'Avenir, and managed by the French National Research Agency (ANR). The authors would like to thank the French Ministry of Environment (DRC 33 and program 190) and ANSES (Nano-data project 2012/2/154, APR ANSES 2012) for financing the work. We are equally grateful to Olivier Aguerre-Chariol, Patrice Delalain, Pauline Molina and Farid Ait-Ben-Ahmad for their cooperation and advice during the experiments.

Supporting Information Available

More details on the materials used during the study can be found in the supporting information. This information is available free of charge via the Internet at http://pubs.acs.org/.

Acknowledgements

[1] Torgal, F.P.; Jalali, S. Eco-efficient construction and building materials. *Constr. Build. Mater.* **2011**, *25*, 582-590.

[2] Stamate, M.; Lazar, G. Application of titanium dioxide photocatalysis to create self-cleaning materials. *Romanian Technical Sciences Academy MOCM* **2007**, 13-3, 280-285.

[3] Vorbau, M.; Hillemann, L.; Stintz, M. Method for the characterization of the abrasion induced nanoparticle release into air from surface coatings. *Aerosol Sci* **2009**, 40, 209-217.

[4] Shandilya, N.; Le Bihan, O.; Morgeneyer, M. A review on the study of the generation of (nano-) particles aerosols during the mechanical solicitation of materials. *J Nanomater* **2014**, Art. ID 289108.

[5] Le Bihan, O.; Shandilya, N.; Gheerardyn, L.; Guillon, O.; Dore, E.; Morgeneyer, M.. Investigation of the Release of Particles from a Nanocoated Product. *Advances in Nanoparticles* **2013**, 2, 39-44.

[6] Göhler, D.; Nogowski, A.; Fiala, P.; Stintz, M. Nanoparticle release from nanocomposites due to mechanical treatment at two stages of the life-cycle. *J Phys Conf Ser* **2013** 429 (2013) 012045; DOI: 10.1088/1742-6596/429/1/012045.

[7] Allen, N.S.; Edge, M.; Corrales, T.; Childs, A.; Liauw, C.M.; Catalina, F.; Peinado, C.; Minihan, A.; Aldcroft, D. Ageing and stabilisation of filled polymers: an overview. *Polym Degrad Stabil* **1998**, 61, 183-199.

[8] Allen, N.S.; Edge, M.; Ortega, A.; Sandoval, G.; Liauw, C.M.; Verran, J.; Stratton, J.; McIntyre, R.B. Degradation and stabilisation of polymers and coatings: nano versus pigmentary titania particles. *Polym Degrad Stabil* **2004**, 85, 927-946.

[9] Hsu, L.Y.; Chein, H.M. Evaluation of nanoparticle emission for TiO_2 nanopowder coating materials. *J Nanopart Res* **2007**, 9, 157-163.

[10] Al-Kattan, A.; Wichser, A.; Vonbank, R.; Brunner, S.; Ulrich, A.; Zuind, S.; Nowack, B. Release of TiO_2 from paints containing pigment-TiO_2 or nano-TiO_2 by weathering. *Env Sci Process Impact* **2013**, 15, 2186-2193.

[11] Kaegi, R.; Ulrich, A.; Sinnet, B.; Vonbank, R.; Wichser, A.; Zuleeg, S.; Simmler, H.; Brunner, S.; Vonmont, H.; Burkhardt, M.; Boller, M. Synthetic TiO_2 nanoparticle emission from exterior facades into the aquatic environment. *Environ Pollut* **2008**, 156, 233-239.

406 [12] Hirth, S.; Cena, L.; Cox, G.; Tomovic, Z.; Peters, T.; Wohlleben, W. Scenarios and
407 methods that induce protruding or released CNTs after degradation of nanocomposite
408 materials. *J Nanopart Res* **2013**, 15, 1504-1518.
409 [13] Wohlleben, W.; Brill, S.; Meier, M. W.; Mertler, M.; Cox, G.; Hirth, S.; von Vacano, B.;
410 Strauss, V.; Treumann, S.; Wiench, K.; Ma-Hock, L.; Landsiedel, R. On the lifecycle of
411 nanocomposites: comparing released fragments and their in vivo hazards from three
412 release mechanisms and four nanocomposites. *Small* **2011**, 7, 2384-2395.
413 [14] Al-Kattan, A.; Wichser, A.; Zuin, S.; Arroyo, Y.; Golanski, L.; Ulrich, A.; Nowack, B.
414 Behavior of TiO2 released from nano-TiO2-containing paint and comparison to pristine
415 nano-TiO_2. *Environmental Science & Technology* **2014**, 48, 6710-6718.
416 [15] Gondikas, A. P.; von der Kammer, F.; Reed, R. B.; Wagner, S.; Ranville, J. F.; Hofmann,
417 T. Release of TiO_2 nanoparticles from sunscreens into surface waters: a one-year survey
418 at the old danube recreational lake. *Environmental Science & Technology* **2014**, 48, 5415-
419 5422.
420 [16] von Goetz, N.; Lorenz, C.; Windler, L.; Nowack, B.; Heuberger, M.; Hungerbuhler, K.
421 Migration of Ag- and TiO_2- (nano)particles from textiles into artificial sweat under
422 physical stress: experiments and exposure modeling. *Environmental Science &*
423 *Technology* **2013**, 47, 9979-9987.
424 [17] Windler, L.; Lorenz, C.; von Goetz, N.; Hungerbuhler, K.; Amberg, M.; Heuberger, M.;
425 Nowack, B. Release of titanium dioxide from textiles during washing. *Environmental*
426 *Science & Technology* **2012**, 46, 8181-8188.
427 [18] Zhang, W.; Crittenden, J.; Li, K. G.; Chen, Y. S.; Attachment efficiency of nanoparticle
428 aggregation in aqueous dispersions: modeling and experimental validation.
429 *Environmental Science & Technology* **2012**, 46, 7054-7062.

[19] Stefano, Z.; Marco, G.; Arlen, F.; Luan, G. Leaching of nanoparticles from experimental water-borne paints under laboratory test conditions. *Journal of Nanoparticle Research* **2013**, 16, 2185.

[20] Petkovic, J.; Zegura, B.; Stevanovic, M.; Drnovsek, N.; Uskokovic, D.; Novak, S. DNA damage and alterations in expression of DNA damage responsive genes induced by TiO_2 nanoparticles in human hepatoma HepG2 cells. *Nanotoxicology* **2011**, 5, 341-353.

[21] Unnithan, J.; Rehman, M.U.; Ahmad, F.J.; Samim, M. Aqueous Synthesis and Concentration-Dependent dermal toxicity of TiO_2 nanoparticles in wistar rats. *Biol Trace Elem Res* **2011**, 143, 1682-1694.

[22] Warheit, D.B.; Brock, W.J.; Lee, K.P.; Webb, T.R.; Reed, K.L. Comparative pulmonary toxicity inhalation and instillation studies with different TiO_2 particle formulations. *Toxicol Sci* **2005**, 88, 514-524.

[23] Yamashita, K.; Yoshioka, Y.; Higashisaka, K.; Mimura, K.; Morishita, Y.; Nozaki, M.; Yoshida, T.; Ogura, T.; Nabeshi, H.; Nagano, K.; Abe, Y.; Kamada, H.; Monobe, Y.; Imazawa, T.; Aoshima, H.; Shishido, K.; Kawai, Y.; Mayumi, T.; Tsunoda, S.; Itoh, N.; Yoshikawa, T.; Yanagihara, I.; Saito, S.; Tsutsumi, Y. Silica and titanium dioxide nanoparticles cause pregnancy complications in mice. *Nat Nanotechnol* **2011**, 6, 321-328.

[24] Barnard, A.S. One-to-one comparison of sunscreen efficacy, aesthetics and potential nanotoxicity. *Nat Nanotechnol* **2010**, 5, 271-274.

[25] Auffan, M.; Rose, J.; Bottero, J.Y.; Lowry, G. V.; Jolivet, J.P.; Wiesner, M. R. Towards a definition of inorganic nanoparticles from an environmental, health and safety perspective. *Nat Nanotechnol* **2009**, 4, 634-641.

[26] AFNOR. Paints and varnishes – Methods of exposure to laboratory light sources – Part 1: General guidance, ISO 16474-1, **2012**.

[27] Morgeneyer, M.; Shandilya, N.; Chen, Y.M.; Le Bihan, O. Use of a modified Taber abrasion apparatus for investigating the complete stress state during abrasion and in-process wear particle aerosol generation. *Chem Eng Res Des*, DOI: http://dx.doi.org/10.1016/j.cherd.2014.04.029

[28] ASTM. International. Standard Test method for the abrasion of organic coatings by the Taber Abradant, ASTM D4060, **2007**.

[29] ASTM. International. Standard Test Methods for Dry Abrasion Mar Resistance of High Gloss Coatings, ASTM D6037, **1996**.

[30] ASTM. International, Standard Test Method for Resistance of Transparent Plastics to Surface Abrasion, ASTM D1044, **2008**.

[31] Golanski, L.; Guiot, A.; Pras, M.; Malarde, M.; Tardif, F. Release-ability of nano fillers from different nanomaterials (toward the acceptability of nanoproduct). *J Nanopart Res* **2012**, 14, 962-970.

[32] Hassan, M.M.; Dylla, H.; Mohammad, L.N.; Rupnow, T. Evaluation of the durability of titanium dioxide photocatalyst coating for concrete pavement. *Constr Build Mater* **2010**, 24, 1456-1461.

[33] Morgeneyer, M.; Le Bihan, O.; Ustache, A.; Aguerre Chariol, O. Experimental study of the aerosolization of fine alumina particles from bulk by a vortex shaker. *Powder Technol* **2013**, 246, 583-589.

[34] Le Bihan, O.; Morgeneyer, M.; Shandilya, N.; Aguerre Chariol, O.; Bressot, C. In *Handbook of Nanosafety- Measurement, Exposure and Toxicology*; Vogel, U., Savolainen, K., Wu, Q., Van Tongeren, M., Brouwer, D., Berges M., Eds.; Academic Press: San Diego **2014**; Ch. 7

[35] Göhler, D.; Stintz, M.; Hillemann, L.; Vorbau, M. Characterization of Nanoparticle Release from Surface Coatings by the Simulation of a Sanding Process. *Ann Occup Hyg* **2010**, 54, 615-624.

[36] R'mili, B.; Le Bihan, O.; Dutouquet, C.; Aguerre Charriol, O.; Frejafon, E. Sampling by TEM Grid Filtration. *Aerosol Sci Tech* **2013**, 47, 767-775.

[37] Shandilya, N.; Le Bihan, O.; Morgeneyer, M., Effect of the normal load on the release of aerosol wear particles during abrasion. *Tribol Lett* **2014**, 55, 227-234.

[38] Brockmann, J.E. In *Aerosol Measurement- Principles, Techniques and Applications*; Kulkarni, P., Baron, P.A., Willeke, K., Eds.; John Wiley & Sons: New Jersey **2011**, Ch. 6.

[39] White, L.R. Capillary rise in powders. *J Colloid Interf Sci* **1982**, 90, 536-538.

[40] Murray, M. Cracking in coatings from colloidal dispersions: An industrial perspective. Proceedings Rideal Lecture, London, 20 April **2009**.

[41] Dufresne, E.R.; Corwin, E.I.; Greenblatt, N.A.; Ashmore, J.; Wang, D.Y.; Dinsmore, A.D.; Cheng, J.X.; Xie, X.S.; Hutchinson, J.W.; Weitz, D.A. Flow and Fracture in Drying Nanoparticle Suspensions. *Phys Rev Lett* **2003**, 91, 224501-1 - 224501-4.

[42] Tirumkudulu, M.S.; Russel, W.B. Cracking in Drying Latex Films. *Langmuir* **2005**, 21, 4938-4948.

[43] Hare, C.H. The Degradation of Coatings by Ultraviolet Light and Electromagnetic Radiation. *Protective Coatings and Linings* **1992**.

[44] Shandilya, N.; Le Bihan, O.; Bressot, C.; Morgeneyer, M. Evaluation of the particle aerosolization from n-TiO_2 photocatalytic nanocoatings under abrasion. *J Nanomater* **2014**, Art. ID 185080.

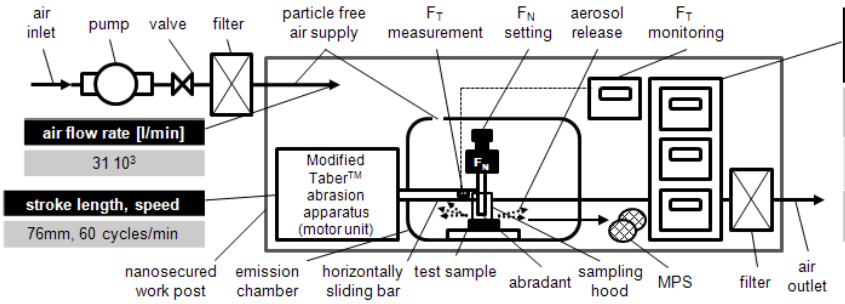

Particle sizing / counting	Instrument TSI	Particle size range [nm]	air flow rate [l/min]	sampl. time [s]
CPC	3775	4 .. 3 10^3	1.5	1
APS	3321	0.5 10^3 .. 20 10^3	5	5
SMPS	DMA 3081, CPC 3775	15 .. 500	0.3	120

Figure 1. Experimental set-up

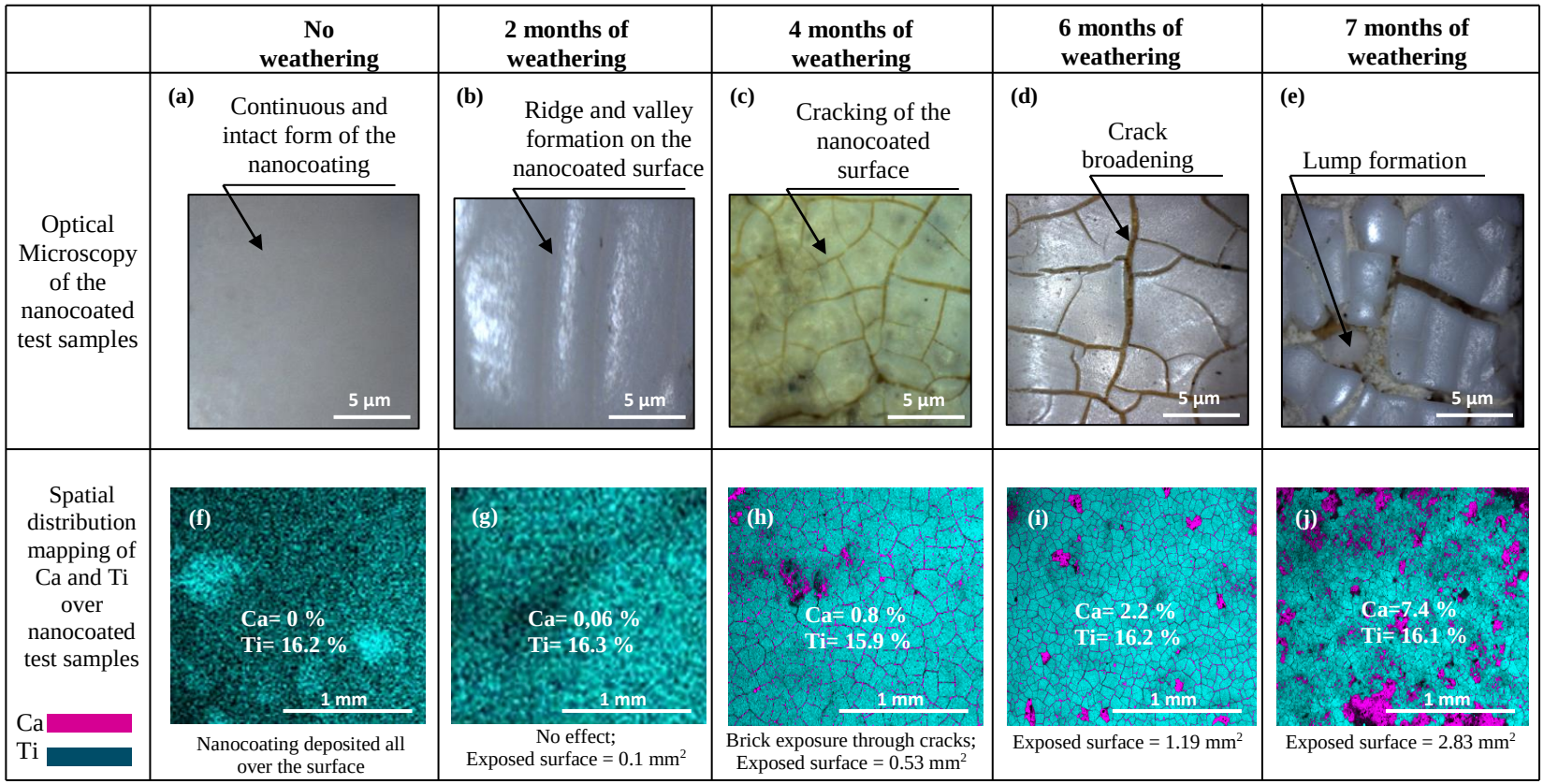

Figure 2. Microscopic analysis of the nanocoated sample

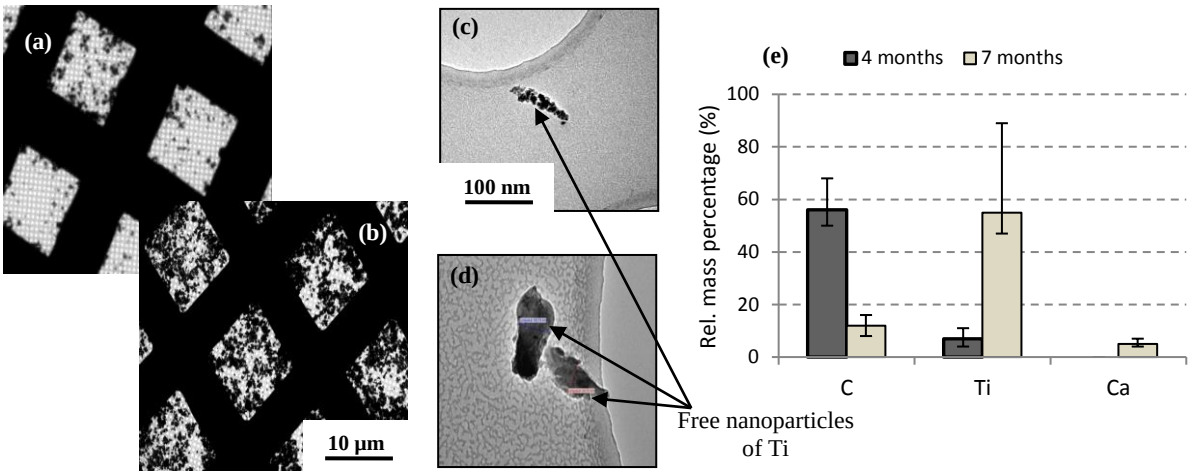

Figure 3. TEM image of the aerosol particles emitted from the abrasion of **(a)** 4 months **(b)** 7 months weathered nanocoated samples **(c)**, **(d)** Free nanoparticles emitted from the abrasion of 7 months weathered nanocoated samples **(e)** Chemical analysis of the aerosol particles emitted from the abrasion of 4 and 7 months weathered nanocoated samples

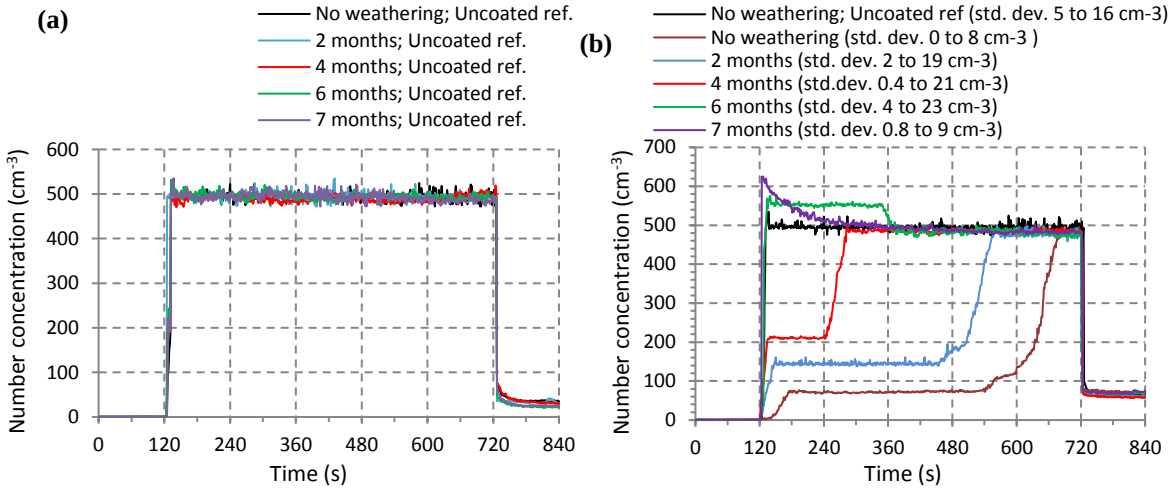

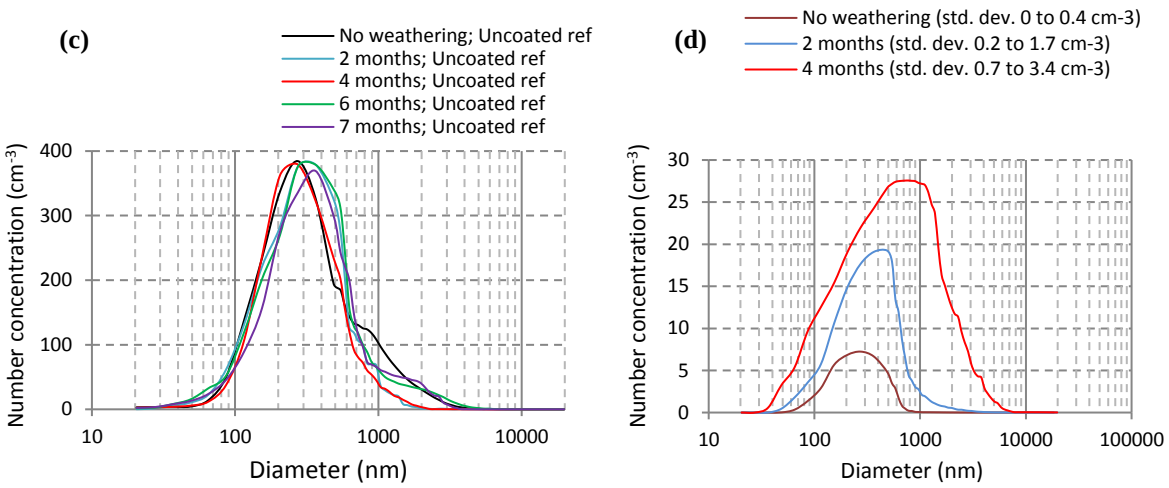

Figure 4. EAPNC during the abrasion of weathered **(a)** uncoated reference sample (**b**) nanocoated samples

PSD of the emitted aerosol particles during the abrasion of weathered **(c)** uncoated reference sample (t= 120 s to 720 s) (**d**) nanocoated samples (corresponding to the phase during which the concentration is constant for the first time in figure 4 (b))

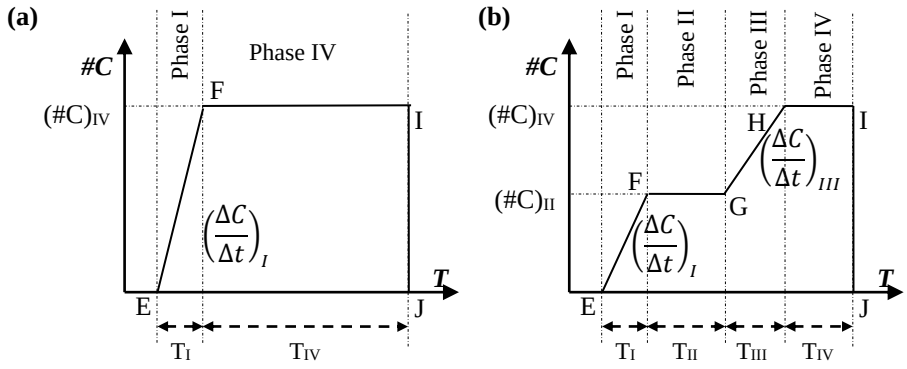

Figure 5. Variation of aerosol particle number concentration generated from **(a)** uncoated and **(b)** nanocoated surface samples

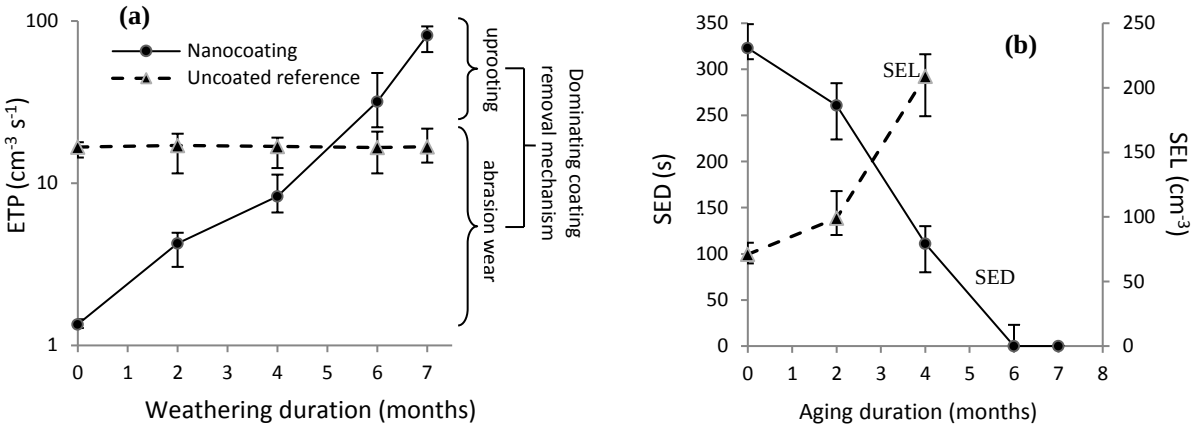

Figure 6. Variation of (**a**) ETP (**b)** SED and SEL with the weathering duration